Latin American Journal of Solids and Structures
www.lajss.org

Calibration and evaluation of the Lemaitre damage model using axial-torsion fatigue tests on five engineering alloys

Abstract
The Lemaitre damage model is evaluated using fatigue test data from five engineering alloys: 1045 steel, 16MnR steel, 7075-T651 Al alloy, extruded AZ61A Mg alloy, and extruded AZ31B Mg alloy. Tension–compression, torsion, proportional axial-torsion, and 90° out-of-phase axial-torsion loadings were investigated. The results show that the overall accuracy of the fatigue life estimates made by using the Lemaitre model is comparable to those obtained by fatigue models that require the definition of a loading cycle. A simple and effective method is described for determining the material constants of the Lemaitre model.

Keywords
Multiaxial fatigue, Life prediction, Damage mechanics, Carbon steel, Aluminum alloy, Magnesium alloy.

Fábio Castro[a]*
Cainã Bemfica[a]

[a] Departamento de Engenharia Mecânica, Universidade de Brasília – UnB, Brasília, DF, Brasil. E-mail: fabiocastro@unb.br, cainabemfica@gmail.com

*Corresponding author.

http://dx.doi.org/10.1590/1679-78254340

Received: July 21, 2017
In Revised Form: January 17, 2018
Accepted: January 19, 2018
Available Online: May 02, 2018

1 INTRODUCTION

Fatigue crack initiation is a primary type of failure in structural members under cyclic loading. Common examples of fatigue critical members include axles, bearings, crankshafts, pressure vessels, and turbine blades. Such members often experience multiaxial stress-strain conditions originated from multiple applied loads and/or notch effects (Socie and Marquis, 2000; Sharifi et al., 2016; Googarchin et al., 2017). In addition, depending on the nature of the applied loads, the cyclic stresses and strains can be proportional or nonproportional, and of constant or varying amplitude.

Many of the multiaxial fatigue life prediction methods that have been developed over the years are based on four components: a constitutive model for the calculation of the cyclic stress-strain response, a fatigue damage parameter, a cycle counting method, and a damage summation rule. A comprehensive overview of the different modeling approaches for each of these four components, including their implications for fatigue life prediction, is presented in the book by Socie and Marquis (2000). A further discussion on these four fundamental issues in multiaxial fatigue is given by Fatemi and Shamsaei (2011).

In parallel to the advances in the traditional methods for fatigue life prediction, progress has also been made in the development of fatigue damage evolution rules for metals (see, e.g., Chow and Wei, 1991; Bonora and Newaz, 1998; Jiang, 2000; Lemaitre and Desmorat, 2005; Jiang et al., 2009; Shen et al., 2015; Lopes and Malcher, 2017). As cycle counting under multiaxial loading conditions is still a difficult task, its elimination in many of the damage evolution rules is an attractive feature. For simplicity, a scalar damage quantity is often used to represent fatigue damage, and, hence, no information on the crack orientation is given. A remarkable exception is the incremental fatigue damage model developed by Jiang (2000), which incorporates the critical plane concept in multiaxial fatigue.

Despite the progress in the formulation of fatigue damage evolution rules, the experimental evaluation of many of such rules has been limited to simple uniaxial loading conditions. However, efforts to evaluate damage models by using multiaxial tests under more complicated loading conditions can be found in some studies (Jiang, 2000; Jiang et al., 2007; Jiang et al., 2009; Castro and Jiang, 2016; Castro and Jiang, 2017). Also, in a recent work by Lopes and Malcher (2017), the Lemaitre damage model has been evaluated with respect to proportional and nonproportional axial-torsion fatigue data.

The damage model developed by Lemaitre (1985) can describe various damage behaviors. Although widely used to estimate ductile fracture, fatigue life prediction based on the Lemaitre model has received much less attention. The experimental evaluation carried out by Lopes and Malcher (2017) indicated that the Lemaitre model

can provide reasonably accurate fatigue lives for three engineering materials (304 stainless steel, S460N steel, and 6061-T6 Al alloy) under proportional and nonproportional, axial-torsion loading conditions. However, very few torsion tests were examined by Lopes and Malcher (3 torsion tests on the S460N steel), and the fatigue tests on the 6061-T6 Al alloy were limited to the low-cycle fatigue regime. It is desirable to evaluate the Lemaitre model using different materials and testing conditions.

In the present work, the Lemaitre damage model is further evaluated based on experimentally observed fatigue lives of five engineering metals: 1045 steel, 16MnR steel, 7075-T651 Al alloy, extruded AZ61A Mg alloy, and extruded AZ31B Mg alloy. A simple and effective method for determining the material constants of the Lemaitre model is also presented.

2 LEMAITRE DAMAGE MODEL

Lemaitre developed a fatigue model for general multiaxial loading based on the framework of continuum thermodynamics (Lemaitre, 1985; Lemaitre and Desmorat, 2005). A scalar quantity, D, is used in this model to describe the fatigue damage at a material point, and a macroscopic crack is predicted to occur when the fatigue damage reaches a critical value, D_c. The damage evolution rule takes the following form:

$$\dot{D} = \left(\frac{Y}{S}\right)^s \dot{p} \tag{1}$$

where S and s are material constants and the superposed dot denotes differentiation with respect to time. The quantity $\dot{p}$ is the equivalent plastic strain rate defined as $\dot{p} = \sqrt{2/3}\left\|\dot{\boldsymbol{\varepsilon}}^p\right\|$, where $\boldsymbol{\varepsilon}^p$ is the plastic strain tensor and the symbol $\|\|$ stands for the Euclidean norm of a second-order tensor. Y is expressed as

$$Y = \frac{\sigma_{\mathrm{eq}}^2 R_\nu}{2E\left(1-D\right)^2} \tag{2}$$

In Eq. (2), E is the Young's modulus, σ_{eq} is the von Mises equivalent stress, and R_ν is a scalar function defined as

$$R_\nu = \frac{2}{3}\left(1+\nu\right) + 3\left(1-2\nu\right)\eta^2 \tag{3}$$

where ν is the Poisson's ratio. The quantity η is called stress triaxiality and is defined as $\eta = \sigma_{\mathrm{h}} / \sigma_{\mathrm{eq}}$, where σ_{h} is the hydrostatic stress.

2.1 Constant amplitude loading

The Lemaitre model is applicable to general multiaxial loading. For any loading history, the occurrence of fatigue failure can be predicted by numerical integration of Eq. (1) until a critical value. For constant amplitude loading, if a stabilized stress–strain response can be identified well before the total number of cycles to failure, a convenient expression for fatigue life prediction can be derived as follows. The fatigue damage increment per loading cycle is given by

$$\frac{\delta D}{\delta N} = \int_{\mathrm{cycle}} \dot{D}\,\mathrm{d}t \tag{4}$$

where, as usual in fatigue damage analysis, the variation of damage with the number of loading cycles is regarded as continuous, and the prefix δ denotes an infinitesimal. Inserting (1) and (2) in (4), and neglecting the variation of D over a cycle, it follows that

$$\frac{\delta D}{\delta N} = \frac{1}{\left(1-D\right)^{2s}} \int_{\mathrm{cycle}} \left(\frac{\sigma_{\mathrm{eq}}^2 R_\nu}{2ES}\right)^s \mathrm{d}p \tag{5}$$

The above relation implies that

$$\left(1-D\right)^{2s}\delta D = I\delta N \tag{6}$$

where

$$I = \int_{\text{cycle}} \left(\frac{\sigma_{\text{eq}}^2 R_v}{2ES} \right)^s \mathrm{d}p \tag{7}$$

The estimated number of cycles to failure, N_{est}, is determined by integrating Eq. (6) over the whole loading history. If the stress–strain response becomes stabilized well before the total number of cycles to failure, the value of I can be regarded as a constant. Thus,

$$\int_0^{D_c} \left(1-D\right)^{2s}\delta D = \int_0^{N_{\text{est}}} I\delta N = IN_{\text{est}} \tag{8}$$

In view of (8), the following formula for fatigue life prediction can be obtained:

$$N_{\text{est}} = \frac{1-\left(1-D_c\right)^{1+2s}}{\left(1+2s\right)I} \tag{9}$$

2.2 Determination of material constants

There are three fatigue-related constants (S , s, D_c) in the Lemaitre model. To determine these constants, the following objective function based on the squared difference between estimated and observed fatigue lives is minimized:

$$\Phi = \sum_{i=1}^{n} \left(\log \frac{N_{\text{est}}^{(i)}}{N_{\text{obs}}^{(i)}} \right)^2 \tag{10}$$

where n is the number of test data used to determine the material constants, the superscript (i) denotes the i th test, $N_{\text{obs}}^{(i)}$ is the observed fatigue life, and $N_{\text{est}}^{(i)}$ is the fatigue life estimated by using Eq. (9). To solve the minimization problem, an exhaustive search over a pre-defined domain of candidate constants is carried out. The method can be readily implemented in a computer and its computational cost is very low.

3 CYCLIC PLASTICITY MODEL

Uncoupling between the elastic-plastic constitutive behavior and fatigue damage is assumed in this paper. Within this framework, the cyclic stress and strain histories at the critical location of the engineering component are first determined by using, for example, a finite element model. Fatigue crack initiation life is then predicted by post-processing the stress-strain data using a fatigue damage model.

The stress-strain analysis was performed in this work by using the cyclic plasticity model developed by Jiang and Sehitoglu (1996a). The basic constitutive relations of the model are summarized in Table 1. The model was chosen due to its reasonable predictions of the stress and strain responses for general multiaxial loading, as demonstrated in previous studies (Jiang and Kurath, 1996, 1997; Socie, 1998).

Strain-controlled axial fatigue testing with solid cylindrical specimens and strain-controlled axial-torsion fatigue testing with thin-walled tubular specimens were evaluated in this work. For such experimental configurations, the axial and/or shear stress distributions can be assumed uniformly distributed over the cross section of the specimen. By taking advantage of this feature, the numerical implementation of the cyclic plasticity model was achieved by developing a MATLAB script that simulates the stress response of a material point under prescribed axial and shear strains. The stress update algorithm was based on an explicit integration scheme.

Table 1: *Summary of the Jiang–Sehitoglu cyclic plasticity model.*

1) Yield function
$f = \| \mathbf{S} - \boldsymbol{\alpha} \|^2 - 2k^2 = 0$
2) Flow rule
$\dot{\boldsymbol{\varepsilon}}^p = \frac{1}{\cdot}\langle \dot{\mathbf{S}} \cdot \mathbf{n} \rangle \mathbf{n}$
3) Hardening rule
$\boldsymbol{\alpha} = \sum_{i=1}^{M} \boldsymbol{\alpha}^{(i)}$ $\dot{\boldsymbol{\alpha}}^{(i)} = c^{(i)} r^{(i)} \left[\mathbf{n} - \left(\frac{\| \boldsymbol{\alpha}^{(i)} \|}{r^{(i)}} \right)^{\chi^{(i)}+1} \frac{\boldsymbol{\alpha}^{(i)}}{\| \boldsymbol{\alpha}^{(i)} \|} \right] \dot{p} \quad (i = 1, 2, ..., M)$

$\mathbf{S}$ = deviatoric stress, $\boldsymbol{\alpha}$ = backstress, k = yield stress in shear, $\mathbf{n}$ = normal on the yield surface, h = plastic modulus function, $\boldsymbol{\varepsilon}^p$ = plastic strain, $\boldsymbol{\alpha}^{(i)} = i$ th backstress part, M = number of backstress parts, $\dot{p}$ = equivalent plastic strain rate, and $c^{(i)}$, $r^{(i)}$, $\chi^{(i)}$ = material constants.

4 RESULTS AND DISCUSSION

The Lemaitre model was evaluated using axial-torsion fatigue test data available in the literature (Fatemi and Stephens, 1989a; Zhao and Jiang, 2008; Gao et al., 2009; Yu et al., 2011; Xiong et al., 2012). Five engineering materials were investigated: normalized 1045 steel, 16MnR steel, 7075-T651 Al alloy, extruded AZ61A Mg alloy, and extruded AZ31B Mg alloy. 1045 steel is a medium carbon steel that is widely used in the ground vehicle industry. 16MnR steel (also designated Q345R steel and similar to ASME SA302B) is usually applied to manufacture pressure vessels. 7075 Al alloys are commonly used in aircraft structures. Wrought magnesium alloys are potential candidates for structural applications in transportation and aerospace industries due to their high strength-to-weight ratio (Bettles and Barnett, 2012).

The loading paths used in the tests are shown in Fig. 1, where ε is the axial strain and γ is the shear strain. Fully reversed tension–compression, fully reversed torsion, proportional (in-phase) loading, and nonproportional (90º out-of-phase) loading were investigated. The test data for 1045 steel were obtained by testing thin-walled tubular specimens (Fatemi and Stephens, 1989a). The experiments on 16MnR steel and 7075-T651 Al alloy were performed by Gao et al. (2009) and Zhao and Jiang (2008), respectively. For these materials, two types of specimens were tested: solid cylindrical specimens for uniaxial loading and thin-walled tubular specimens for torsion and axial-torsion. For the AZ61A and AZ31B Mg alloys, thin-walled tubular specimens were used for all tests (Yu et al., 2011; Xiong et al., 2012). Further details of the fatigue tests used in this work, including the test setup, specimen dimensions, and cracking orientations, can be found in the corresponding references.

Failure was defined by a load drop criterion in most of the experiments (5% load drop for the 16MnR steel, AZ61A Mg alloy, and AZ31B Mg alloy, and 10% load drop for the 1045 steel and 7075-T651 Al alloy), the exception being the uniaxial solid specimens of 7075-T651 Al alloy, which were tested to complete fracture. For the materials, loading conditions, and specimen geometries studied, the crack propagation phase was expected to be a small part of the total life.

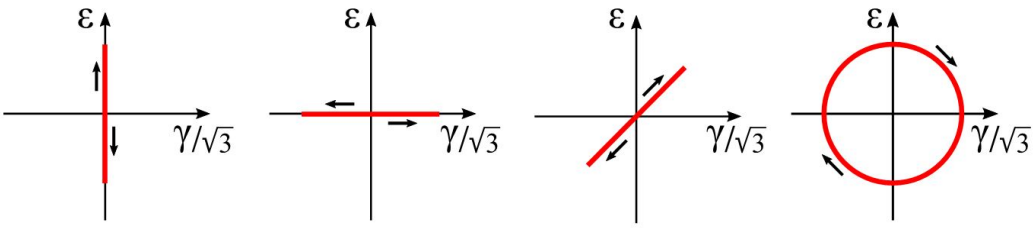

Figure 1: *Loading paths used in the fatigue tests.*

Fatigue life prediction by the Lemaitre model requires as input the stress–strain hysteresis loops at the critical material point. For the AZ61A and AZ31B Mg alloys, the stress–strain loops obtained directly from the fatigue tests were available to the authors. On the other hand, for the 1045 steel, 16MnR steel, and 7075-T651 Al alloy, the stresses and strains were simulated by using the Jiang–Sehitoglu plasticity model. The material constants of the model were determined from the uniaxial cyclic stress-strain curve by using the method described by Jiang and Sehitoglu (1996b). The format of the cyclic stress-strain curve was described by the Ramberg–Osgood relationship. Table 2 lists the material constants used in this study for the Jiang–Sehitoglu model.

Table 2: *Material constants used in the Jiang–Sehitoglu plasticity model.*

1045 steel
E = 204 GPa, $\nu = 0.27$, $k = 50$ MPa
$c^{(1)} = 12583.2$, $c^{(2)} = 1859.5$, $c^{(3)} = 475.2$, $c^{(4)} = 164.4$, $c^{(5)} = 68.9$
$r^{(1)} = 55.8$, $r^{(2)} = 56.0$, $r^{(3)} = 55.0$, $r^{(4)} = 54.5$, $r^{(5)} = 116.3$
$\chi^{(1)} = \chi^{(2)} = \cdots = \chi^{(5)} = 5$
16MnR steel
E = 212.5 GPa, $\nu = 0.31$, $k = 50$ MPa
$c^{(1)} = 18373.8$, $c^{(2)} = 1721.7$, $c^{(3)} = 325.3$, $c^{(4)} = 89.8$, $c^{(5)} = 31.5$
$r^{(1)} = 67.8$, $r^{(2)} = 65.9$, $r^{(3)} = 64.4$, $r^{(4)} = 63.7$, $r^{(5)} = 116.5$
$\chi^{(1)} = \chi^{(2)} = \cdots = \chi^{(5)} = 5$
7075-T651 Al alloy
E = 71.7 GPa, $\nu = 0.3$, $k = 100$ MPa
$c^{(1)} = 651313.5$, $c^{(2)} = 121390.2$, $c^{(3)} = 29596.0$, $c^{(4)} = 8764.4$, $c^{(5)} = 3007.4$
$c^{(6)} = 1158.2$, $c^{(7)} = 489.5$, $c^{(8)} = 223.3$, $c^{(9)} = 108.6$, $c^{(10)} = 55.8$
$r^{(1)} = 28.8$, $r^{(2)} = 33.9$, $r^{(3)} = 33.7$, $r^{(4)} = 33.6$, $r^{(5)} = 33.5$
$r^{(6)} = 33.4$, $r^{(7)} = 33.4$, $r^{(8)} = 33.3$, $r^{(9)} = 33.3$, $r^{(10)} = 76.8$
$\chi^{(1)} = \chi^{(2)} = \cdots = \chi^{(10)} = 10$

For all the fatigue experiments, the number of cycles to failure was estimated by using Eq. (9). To obtain the stabilized stresses and strains for the 1045 steel, 16MnR steel, and 7075-T651 Al alloy, elastic-plastic simulations were carried out for 5 loading cycles, and the results at the 5th loading cycle were used to determine the fatigue life. For the AZ61A and AZ31B Mg alloys, the stress-strain hysteresis loops taken from the tests at approximately half the observed fatigue lives were used in Eq. (9). The constants of the Lemaitre model were determined by a least-squares fitting of the tension–compression and torsion data, as described in Section 2.2, and are listed in Table 3.

Table 3: *Material constants used in the Lemaitre damage model.*

Material	S (MPa)	s	D_c
1045 steel	2.1	2.8	0.4
16MnR steel	2.0	2.7	0.8
AZ61A Mg alloy	2.2	1.8	0.1
AZ31B Mg alloy	1.7	2.1	0.1
7075-T651 Al alloy	14.0	0.8	1.0

Observed fatigue lives and estimates made with the Lemaitre model are compared in Figs. 2-4 for the five materials investigated. A data point with a horizontal arrow denotes a run-out test. The solid diagonal lines in these figures represent a perfect correlation, the two dashed lines mark the factor-of-two boundaries in Figs. 2 and 3, and the two dot lines in Fig. 4 are the factor-of-five boundaries.

Most of the fatigue life estimates by the Lemaitre model for the 1045 steel and the 16MnR steel were within the factor-of-two boundaries, indicating that the overall accuracy of the model is excellent. Such accuracy is similar to those obtained by fatigue models based on the critical plane approach (Fatemi and Socie, 1988; Gao et al., 2009). One factor that contributed to such successful fatigue life predictions is the capability of the Jiang–Sehitoglu plasticity model to provide reasonable cyclic stresses and strains. Tables 4 and 5 summarize the accuracy of the elastic-plastic stress-strain analysis carried out for the proportional and nonproportional (90º out-of-phase) axial-torsion tests.

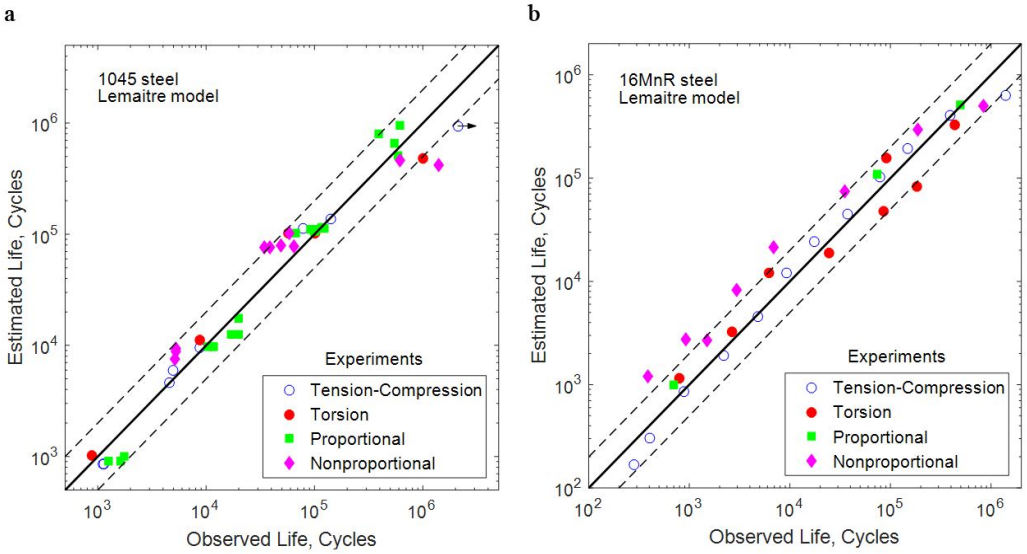

Figure 2: *Observed live versus estimated live for 1045 steel (a) and 16MnR steel (b).*

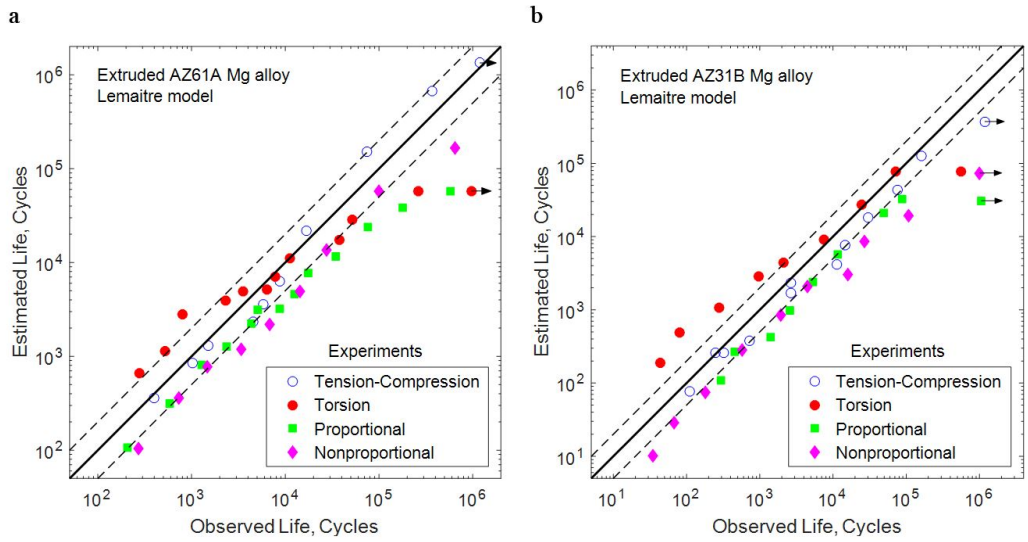

Figure 3: *Observed live versus estimated live for AZ61 Mg alloy (a) and AZ31B Mg alloy(b).*

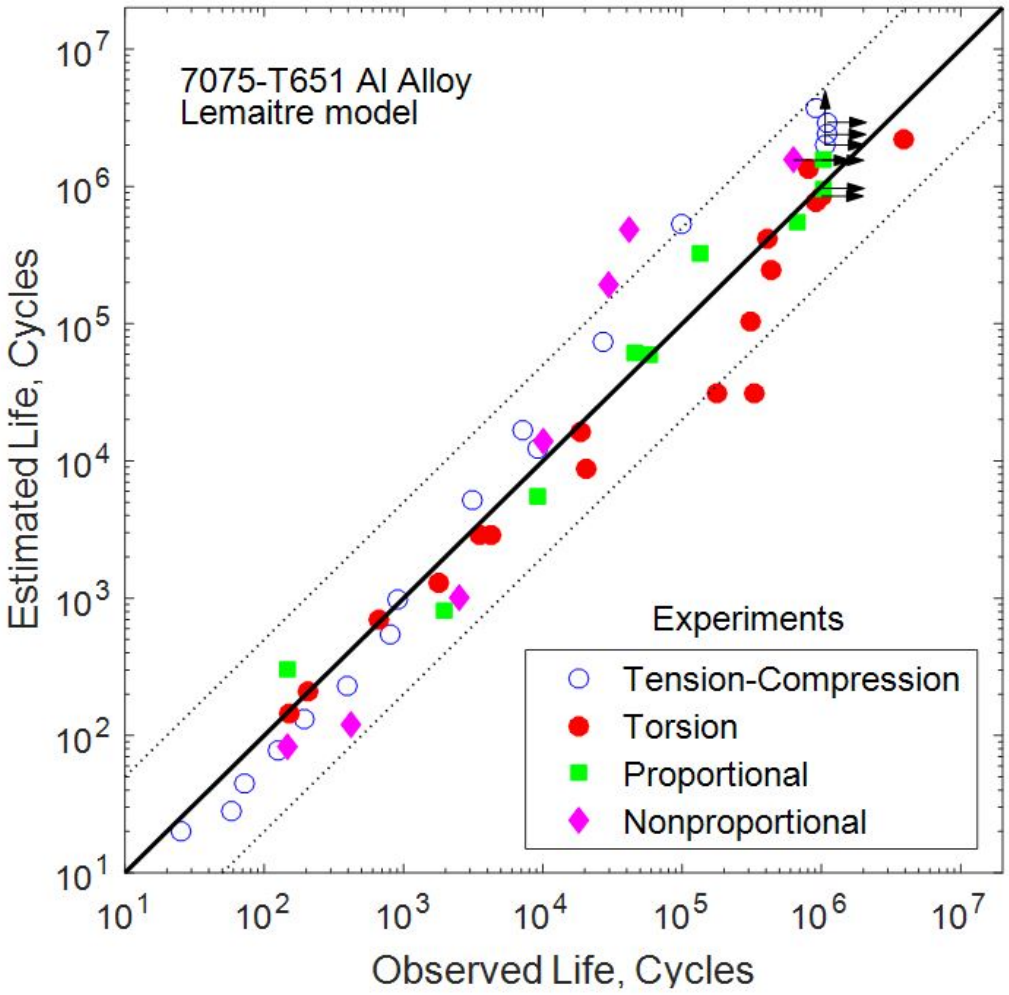

Figure 4: *Observed live versus estimated live for 7075-T651 Al alloy.*

In these tables, the symbols $\Delta\sigma^{exp}$ and $\Delta\tau^{exp}$ refer to the axial and shear stress ranges of the half-life (or near half-life) stress-strain hysteresis loop obtained from the fatigue experiments, while the symbols $\Delta\sigma^{num}$ and $\Delta\tau^{num}$ are the corresponding quantities calculated from numerical simulations using the Jiang-Sehitoglu plasticity model. The results shown in Tables 4 and 5 indicate that the correlation between the experimentally obtained and the simulated stress ranges are better for the proportional than for the nonproportional tests. This is because the adopted plasticity model does not consider the nonproportional hardening effect. However, this effect is not very significant for the two steels studied (Fatemi and Stephens, 1989b; Jiang and Kurath, 1996; Gao et al., 2009), and therefore the overall accuracy of the estimated fatigue lives is good. For the nonproportional tests with fatigue lives less than 10^4 cycles, it can also be noticed that the life estimates for the 1045 steel are better than those obtained for the 16MnR steel (4 data points above the upper factor-of-two boundary). This is due to a better agreement between the experimentally obtained and the simulated stress ranges for the 1045 steel.

Table 4: *Difference between stabilized stress ranges obtained from fatigue experiments on 1045 steel and from numerical simulations using the Jiang-Sehitoglu plasticity model.*

Loading type	Specimen ID	$\frac{\Delta\sigma^{exp}-\Delta\sigma^{num}}{\Delta\sigma^{exp}}$ (%)	$\frac{\Delta\tau^{exp}-\Delta\tau^{num}}{\Delta\tau^{exp}}$ (%)
In-phase axial-torsion	4524	0	5
	4523	0	6
	4528	-2	3
	4516	0	8
	4519	0	7
	4525	0	-3
	4520	1	-4
	4515	2	-1
	4550	0	4
	4514	2	2
	4554	1	0
	4517	2	3
	4526	3	-3
	4503	7	-3
	4501	6	-3
	4522	3	-2
	4548	3	-2
	4521	0	-1
	4509	9	-5
	4530	4	-3
90º out-of-phase axial-torsion	45A3	8	18
	4583	5	4
	4580	18	18
	45B2	14	18
	4586	13	16
	45A5	8	6
	45D4	21	14
	45D1	13	14
	45B5	20	13
	4588	8	5

Although the Lemaitre model can provide reasonable fatigue life predictions for the AZ61A and AZ31B Mg alloy, its performance is not as good as that for the two steels studied. It is found that the model yields somewhat non-conservative life estimates for the proportional and nonproportional tests. Also, the model has a difficult to correlate the torsion tests. It is noted that for the tension–compression and torsion tests, the triaxiality function is a constant and, therefore, the fatigue damage in the Lemaitre model depends only on the von Mises equivalent measures of stress and plastic strain. Thus, the significant difference between the cyclic stress-plastic strain curves of extruded Mg alloys under tension–compression and torsion (Zhang et al., 2011) may have contributed to the less satisfying life predictions for the torsion tests.

Table 5: *Difference between stabilized stress ranges obtained from fatigue experiments on 16MnR steel and from numerical simulations using the Jiang-Sehitoglu plasticity model.*

Loading type	Specimen ID	$\frac{\Delta\sigma^{exp}-\Delta\sigma^{num}}{\Delta\sigma^{exp}}$ (%)	$\frac{\Delta\tau^{exp}-\Delta\tau^{num}}{\Delta\tau^{exp}}$ (%)
In-phase axial-torsion	TU20N	6	6
	TU21N	4	2
	TU09N	13	19
	TU15N	17	21
	TU06S	22	23
	TU09S	23	23
90º out-of-phase axial-	TU07S	32	32
	TU08N	31	29
	TU06N	28	26
	TU03N	30	28
	TU14N	29	32

Observed life versus predicted life for the 7075-T651 Al alloy is shown in Fig. 4. Most of the fatigue life estimates are within the factor-of-five boundaries. The overall accuracy of the Lemaitre model for the 7075-T651 Al alloy is comparable to the scatter of the baseline fatigue data obtained from tension–compression tests (Zhao and Jiang, 2008). Plastic strains in Al alloys are typically very small for fatigue lives higher than 10^4 cycles and, therefore, high-cycle fatigue life prediction is a difficulty for any fatigue model that incorporates plastic strains. To enable the Lemaitre model to be applicable to high-cycle fatigue life prediction of Al alloy, a small yield stress close to the endurance limit under uniaxial loading (Jiang and Kurath, 1996) was used to simulate the small cyclic plastic strains in the material.

5 FURTHER DISCUSSION

The Lemaitre model was used in a previous work by Lopes and Malcher (2017) to estimate fatigue life under axial-torsion loading conditions. The golden-section search was adopted by these authors to determine the damage strength material parameter, S , while maintaining fixed the values for D_c and S ($D_c = 1$, $S = 1$). In the current work, the three constants (S , S, D_c) were determined by simply performing an exhaustive search over a range of candidate constants. No pre-defined values for D_c and S were assumed. Based on the experience gained from the five engineering metals studied, the fatigue constants in the Lemaitre model are generally within the ranges $0 \leq S \leq 14$, $0 \leq S \leq 3$, and $0 \leq D_c \leq 1$. It is also worth mentioning that the evaluation of the fatigue life by Eq. (9) eliminates the need to numerically integrate the damage evolution rule until a critical value, and, hence, the determination of the material constants by an exhaustive search can be performed quickly on a computer. Another advantage of Eq. (9) is that it can be applied to stress–strain hysteresis loops of any shape.

In the fatigue damage analysis performed in this work, no coupling between the stress-strain behavior and the damage was considered. This study and many others (see, e.g., Socie, 1998; Gao et al., 2010) indicate that reasonable fatigue life predictions of conventional metallic materials can be made using an uncoupled procedure if an accurate plasticity model is employed. On the other hand, for materials such as porous sintered metals (Ma and Yuan, 2017) and concrete or for metallic materials under large plastic strains, a coupled analysis is required because of the strong coupling between the stress-strain behavior and the damage in the material.

The material constants of a multiaxial fatigue model are often determined by using test data from tension–compression and torsion tests. Alternatively, the material constants in the Lemaitre model were also determined in the present work by fitting only the tension–compression data. It was found that the fatigue life predictions for the five materials investigated were not significantly altered as compared to the fatigue life estimates shown in Figs. 2-4. Such feature of the Lemaitre model may be useful when only uniaxial fatigue data are available to the design engineer.

A glance at Figs. 2 and 4 shows that the Lemaitre model can correlate well the torsion data of the two steels and of the Al alloy, while the accuracy of the life estimates for the torsion tests on Mg alloys is not so good. An

attempt to improve the life estimates for such torsion data was carried out by relating the damage strength material parameter, S , to the stress triaxiality using a linear relationship,

$$S(\eta) = 3\left(S_{0.33} - S_0\right)|\eta| + S_0 \tag{11}$$

where S_0 and $S_{0.33}$ are material constants. For cyclic torsion $\eta = 0$ and $S = S_0$, whereas for tension–compression $\eta = 0.33$ and $S = S_{0.33}$. To determine the four material constants (S_0, $S_{0.33}$, S, D_c) in the modified Lemaitre model, the method described in Section 2.2 was applied to a dataset obtained from tension–compression and torsion tests. Note that in the numerical computation of the integral that defines the value of *I*, Eq. (7), the expression for $S(\eta)$ in Eq. (11) must be adopted. Figure 5 shows the fatigue lives predicted by the modified Lemaitre model versus the observed fatigue lives for the AZ31B Mg alloy. A significant improvement in the correlation of the torsion data was obtained as compared to the estimates by the original model (refer to Fig. 3b). The overall accuracy of the life predictions for the proportional and nonproportional tests was maintained, except for the nonproportional test with observed life $N_f = 35$ cycles. For AZ61A Mg alloy, the fatigue life estimates based on the original Lemaitre model and its modified version were identical.

The use of a damage strength material parameter as function of the stress triaxiality, Eq. (11), to improve the correlation of tests with different levels of stress triaxiality was inspired by the work of Malcher and Mamiya (2014), in which a modification of the damage strength material parameter yielded better results for ductile fracture prediction. Such a modification of the original Lemaitre model requires an appropriate generalization of the damage potential function. Following the standard formulation of continuum elastic-plastic damage mechanics (Lemaitre and Desmorat, 2005), the damage potential function can be obtained by integrating the damage evolution law with respect to the thermodynamic force associated to the damage, Y . This gives the following expression for the damage potential function:

$$\psi_D = \frac{S(\eta)}{(1-D)(s+1)}\left[\frac{Y}{S(\eta)}\right]^{s+1} \tag{12}$$

where the function $S(\eta)$ is defined by Eq. (11).

For constant amplitude loading and when the stabilized stress–strain response is reached well before the total number of cycles to failure, the fatigue life estimated by the Lemaitre model can be calculated by using Eq. (9). There are cases, however, where the stress response of the material never becomes stabilized. For example, the 1045 steel under high strain amplitude experiences hardening followed by a mild softening for a short period and then a second hardening stage until failure (Fatemi and Stephens, 1989b). Fatigue life prediction based on Eq. (9) can still be used in such cases by taking the stress–strain hysteresis loop at a reference number of cycles (for example, at half of the fatigue life). The results in the present study indicate that such an engineering solution can provide fatigue life estimates with acceptable accuracy. For more general loadings, the variation of the fatigue damage with time (or loading cycle) can be calculated by numerically integrating Eq. (1) or Eq. (5).

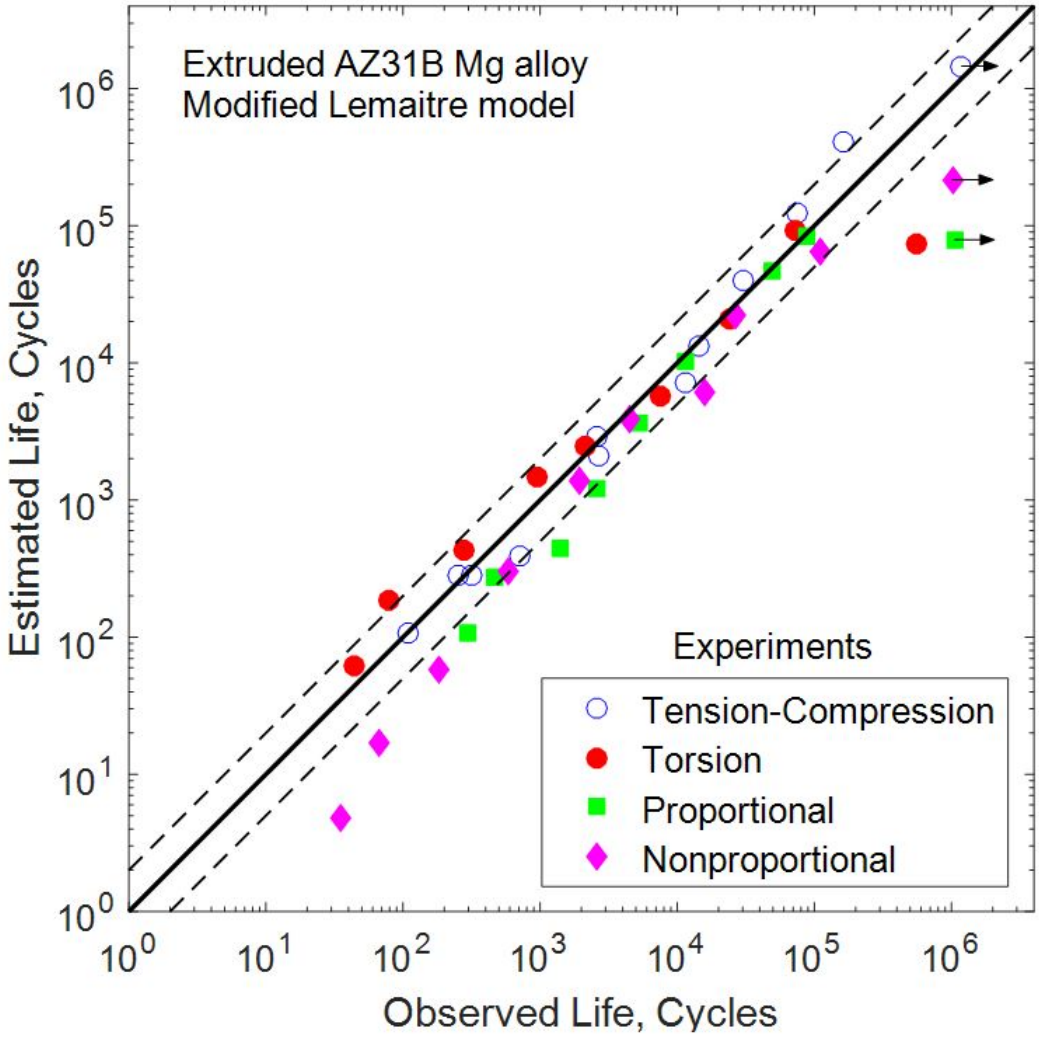

Figure 5: *Observed live versus estimated live based on the modified Lemaitre model for AZ31B Mg alloy.*

The limited stress states that were employed to evaluate the Lemaitre model may have contributed to its good correlation of the fatigue lives. Thin-walled tubular specimens under axial-torsion loading inherently experience limited values of stress triaxiality. Indeed, for any axial-torsion stress state, the stress triaxiality lies in the range $0 \le |\eta| \le 1/3$ because whenever $\sigma \neq 0$ the denominator of the expression for the stress triaxiality, $\eta = 1/3\sigma / \sqrt{\sigma^2 + 3\tau^2}$, is always equal or greater than $|\sigma|$. Since the constants of the modified Lemaitre model were determined by using fatigue data with $\eta = 0$ (torsion tests) and $|\eta| = 1/3$ (tension–compression tests), this may have contributed to the good life estimates. Fatigue experiments covering a wide range of stress triaxiality are needed to better evaluate the modified Lemaitre model.

6 CONCLUSIONS

The Lemaitre damage model was experimentally evaluated using axial-torsion fatigue data of five engineering metals. For 1045 steel, 16MnR steel, and 7075-T651 Al alloy, the Lemaitre model provided life predictions with an accuracy comparable to the scatter of the baseline fatigue tests conducted under tension–compression and torsion (within a factor of 2 for the two steels and within a factor of 5 for the Al alloy). Reasonably accurate fatigue life estimates were also obtained for the AZ61A Mg alloy and the AZ31B Mg alloy, but the model was not able to correlate well some of the torsion tests. A significant improvement in the correlation of the torsion data was

achieved by a modified Lemaitre model in which the damage strength material parameter depends on the stress triaxiality.

Acknowledgments

The authors would like to thank the support provided by CNPq (contracts 308126/2016-5 and 131847/2017-1).

References

Bettles, C., Barnett, M., (Eds.) (2012). Advances in wrought magnesium alloys: Fundamentals of processing, properties and applications. Publisher: Woodhead Publishing.

Bonora, N., Newaz, G. M., (1998). Low cycle fatigue life estimation for ductile metals using a nonlinear continuum damage mechanics model. International Journal of Solids and Structures, 35(6): 1881–1894.

Castro, F., Jiang, Y., (2016). Fatigue life and early cracking predictions of extruded AZ31B magnesium alloy using critical plane approaches. International Journal of Fatigue, 88: 236–246.

Castro, F., Jiang, Y., (2017). Fatigue of extruded AZ31B magnesium alloy under stress- and strain-controlled conditions including step loading. Mechanics of Materials, 108: 77–86.

Chow, C. L., Wei, Y., (1991). A model of continuum damage mechanics for fatigue failure. International Journal of Fracture, 50: 301–316.

Fatemi, A., Shamsaei, N., (2011). Multiaxial fatigue: An overview and some approximation models for life estimation. International Journal of Fatigue, 33: 948–958.

Fatemi, A., Socie, D., (1988). A critical plane approach to multiaxial fatigue damage including out-of-phase loading. Fatigue & Fracture of Engineering Materials and Structures, 11(3): 149–165.

Fatemi, A., Stephens, R. I., (1989a). Biaxial fatigue of 1045 steel under in-phase and 90 deg out-of-phase loading conditions, Multiaxial Fatigue: Analysis and Experiments, Chapter 9, SAE AE-14, 121–137.

Fatemi, A., Stephens, R. I., (1989b). Cyclic deformation of 1045 steel under in-phase and 90 deg out-of-phase axial-torsional loading conditions, Multiaxial Fatigue: Analysis and Experiments, Chapter 10, SAE AE-14, 139–147.

Gao, Z., Zhao, T., Wang, X., Jiang, Y., (2009). Multiaxial fatigue of 16MnR steel. Journal of Pressure Vessel Technology, 131(2): 021403-1–021403-9.

Gao, Z., Qiu, B., Wang, X., Jiang, Y., (2010). An investigation of fatigue of a notched member. International Journal of Fatigue, 32: 1960–1969.

Googarchin, H. S., Sharifi, S. M. H., Forouzesh, F., Hosseinpourd, G. H. R., Etesamia, S. M., Malek Zadea, S. (2017). Comparative study on the fatigue criteria for the prediction of failure in engine structure. Engineering Failure Analysis, 79: 714–725.

Jiang, Y., (2000). A fatigue criterion for general multiaxial loading. Fatigue & Fracture of Engineering Materials and Structures, 23: 19–32.

Jiang, Y., Hertel, O., Vormwald, M., (2007). An experimental evaluation of three critical plane multiaxial fatigue criteria. International Journal of Fatigue, 29: 1490–1502.

Jiang, Y., Kurath, P., (1996). Characteristics of the Armstrong-Frederick type plasticity models. International Journal of Plasticity, 12(3): 387–415.

Jiang, Y., Kurath, P., (1997). Nonproportional cyclic deformation: critical experiments and analytical modeling. International Journal of Plasticity, 13: 743–763.

Jiang, Y., Ott, W., Baum, C., Vormwald, M., Nowack, H., (2009). Fatigue life predictions by integrating EVICD fatigue damage model and an advanced cyclic plasticity theory. International Journal of Plasticity, 25: 780–801.

Jiang, Y., Sehitoglu, H., (1996a). Modeling of cyclic ratchetting plasticity, Part I: development of constitutive equations. ASME Journal of Applied Mechanics, 63: 720–725.

Jiang, Y., Sehitoglu, H., (1996b). Modeling of cyclic ratchetting plasticity, Part II: comparison of model simulations with experiments. ASME Journal of Applied Mechanics, 63: 726–733.

Lemaitre, J., (1985). Coupled elasto-plasticity and damage constitutive equations. Computer Methods in Applied Mechanics and Engineering 51:31–49.

Lemaitre, J., Desmorat, R., (2005). Engineering Damage Mechanics: Ductile, Creep, Fatigue and Brittle Failures. Springer Science & Business Media.

Lopes, J. P., Malcher, L., (2017). Fatigue life estimates under non-proportional loading through continuum damage evolution law. Theoretical and Applied Fracture Mechanics, 88: 64–73.

Ma, S., Yuan H., (2017). A continuum damage model for multi-axial low cycle fatigue of porous sintered metals based on the critical plane concept. Mechanics of Materials, 104: 13–25.

Malcher, L., Mamiya E. N., (2014). An improved damage evolution law based on continuum damage mechanics and its dependence on both stress triaxiality and the third invariant. International Journal of Plasticity, 56: 232–261.

Sharifi, S. M. H., Googarchin, H. S., Forouzesh, F., (2016). Three dimensional analysis of low cycle fatigue failure in engine part subjected to multi-axial variable amplitude thermomechanical load. Engineering Failure Analysis, 62: 128–141.

Shen, F., Voyiadjis, G. Z., Hu, W., Meng, Q., (2015). Analysis on the fatigue damage evolution of notched specimens with consideration of cyclic plasticity. Fatigue & Fracture of Engineering Materials and Structures, 38: 1194–1208.

Socie, D. F., (1998). An evaluation of methods for estimating fatigue damage under multiaxial nonproportional variable amplitude loading. In: Low Cycle Fatigue and Elasto-Plastic Behavior of Materials, Eds. K.T. Rie and P.D. Portella, 205–210.

Socie, D. F., Marquis, G. B., (2000). Multiaxial Fatigue, SAE International, Warrendale.

Xiong, Y., Yu, Q., Jiang, Y., (2012). Multiaxial fatigue of extruded AZ31B magnesium alloy. Materials Science and Engineering: A, 546: 119–128.

Yu, Q., Zhang, J., Jiang, Y., Li, Q., (2011). Multiaxial fatigue of extruded AZ61A magnesium alloy. International Journal of Fatigue, 33(3): 437–447.

Zhang, J., Yu, Q., Jiang, Y., Li, Q., (2011). An experimental study of cyclic deformation of extruded AZ61A magnesium alloy. International Journal of Plasticity, 27: 768–447.

Zhao, T., Jiang, Y., (2008). Fatigue of 7075-T651 aluminum alloy. International Journal of Fatigue, 30: 834–849.